Dynamic dielectric susceptibility of the betaine phosphate (0.15) betaine phosphite (0.85) dipolar glass

J. Banys, S. Lapinskas, and A. Kajokas
Faculty of Physics, Vilnius University, Saulėtekio 9, 2040 Vilnius, Lithuania

A. Matulis
Semiconductor Physics Institute, Goštauto 11, 2600 Vilnius, Lithuania

C. Klimm and G. Völkel
Fakultät für Physik und Geowissenschaften, Universität Leipzig, D-04103 Leipzig, Germany

A. Klöpperpieper
Fakultät für Physik, Universität des Saarlandes, D-66123 Saarbrücken, Germany
(Received 21 January 2002; published 31 October 2002)

Dielectric susceptibility measurements in a wide frequency spectrum were used to obtain the distribution of relaxation times. This was performed by solving the integral equation for the susceptibility with the Tikhonov regularization technique. This method allows to extract the distribution of the relaxation times and resolves multiple dynamical processes. As an experimental example the investigation on mixed crystals of protonated and deuterated $BP_{1-x}BPI_x$ with $x=0.85$ are presented. The dipole-freezing phenomena results in a broad asymmetrical distribution of the relaxation times. The parameters of the double-well potentials of the hydrogen bonds, the local polarization distribution function and the glass order parameter have been extracted from the dielectric measurements. The microscopic parameters obtained are in good agreement with magnetic resonance data.

DOI: 10.1103/PhysRevB.66.144113 PACS number(s): 77.22.Gm, 02.30.Rz, 64.70.Pf, 77.84.Fa

I. INTRODUCTION

The dynamics of the dielectric response of ferroelectrics and related materials is of interest for applications in high-frequency electronic devices, such as static memories, sensors, microstrip lines, etc. Broadband dielectric spectroscopy is widely used to study polarization dynamics in complex systems such as glass-forming liquids and liquid crystalline materials (e.g., Ref. 1). The polarization of a sample in an external electric field depends both on sample geometry and on the mobility of molecular segments, molecules, or clusters of molecules. From the dielectric response one can obtain dipolar strengths, and relaxation processes present in the system. It is common to describe the dynamics in terms of the Debye model, where the exponential temporal decay of the fluctuation with some relaxation time is assumed. However, the dielectric properties of condensed matter do not in general follow the Debye model, thus in order to account for the actual behavior of solids, a distributions of relaxation times have been introduced. In practice, various predefined spectral functions have been used, i.e., single-parameter Cole-Cole, Davidson-Cole, Williams-Wats, and two-parameter Havriliak-Negami, Jonsher, Dissado Hill etc.[1] Typically, a superposition of several such functions provides a satisfactory multiparameter fit to the experimental data. However, it is not always straightforward to relate the obtained parameters to the intrinsic physical properties of the material. A further drawback of such an approach is the inherent difficulty of separating processes with comparable relaxation times. A proper choice of the number of processes used to fit the data is not always obvious, and additional *a priori* assumptions have to be made. An alternative way to describe a dielectric relaxation spectrum is that in terms of an ensemble of Debye processes with a continuous relaxation time distribution $w(\tau)$. For the Debye dispersion $w(\tau)$ reduces to a δ function, while the superposition methods correspond to line shapes with several symmetrically or asymmetrically broadened peaks of $w(\tau)$. Unfortunately, direct extraction of $w(\tau)$ from $\varepsilon^*(\nu)$ is a mathematically ill-posed problem.[2] This difficulty may be one of the reasons why the spectra are usually treated as superpositions of a few parametrized functions. Only few attempts were made to obtain the distribution of relaxation times.[3–5] This method so far has not been applied for the dipolar glasses. Only in Ref. 4 authors tried to obtain the distribution of the relaxation times, but have used empirical functions, what narrowed the problem. If a direct calculation of $w(\tau)$ from ε^* could be reliably performed, in a manner similar to the Fourier transformation between time and frequency domains, then several problems arising from the use of empirical functions could be avoided. Having obtained $w(\tau)$ one could then seek a physical interpretation in the τ domain rather than in the frequency domain. Attempts to develop a suitable numerical algorithm have been made previously[3–5] (and therein).

Among the examples of materials with a broad distribution of relaxation times are dipolar glasses, such as rubidium ammonium dihydrogen phosphate (RADP) or betaine phosphate-phosphite (BP/BPI) mixed crystals.[6–8]

Our purpose is to show that the information obtained from the distribution function of the relaxation times can give better insight into the dynamics of the glassy state.

In this paper, we will concentrate on the BP/BPI mixed

crystals. Betaine phosphate [BP: $[CH_3)_3NCH_2COOH_3PO_4]$ and betaine phosphite (BPI: $[CH_3)_3NCH_2COOH_3PO_3]$ are molecular crystals consisting of the amino-acid betaine as the organic component, and phosphoric and phosphorous acids, respectively, as the inorganic component. In both compounds, the inorganic components (PO_4 or PO_3 groups), linked by hydrogen bonds, form quasi-one-dimensional chains.[9–11] Betaine phosphate shows three phase transitions. It undergoes the first phase transition from a paraelectric high-temperature phase (space group $P2_1/m$; $Z=2$) at 365 K into an antiferrodistortive phase ($P2_1/c; Z=4$) and the second one into an antiferroelectric phase at 86 K ($P2_1/c; Z=8$),[12] the third occours at 81 K. In the high-temperature phase the PO_4 groups and betaine molecules are disordered. They both order in the antiferrodistortive phase, but the hydrogen atoms linking PO_4 groups remain disordered. Ordering of these hydrogen atoms induces the phase transition at 86 K[12] to the antiferroelectric phase.[10] The origin of the third phase transition is not yet known. Deuterated BP (DBP) shows only two phase transitions at 365 and 119 K.[13] The structure of BPI was determined from x-ray and elastic neutron scattering experiments.[9] The x-ray investigation confirmed the structural affinity to BP. It was found that BPI at room temperature is monoclinic (space group $P2_1/c$). BPI crystals show two phase transitions: from the paraelectric $P2_1/m$ high-temperature phase into an antiferrodistortive $P2_1/c$ phase at $T_{C1}=355$ K with a unit cell doubling along c axis and an order-disorder transition of the hydrogen bond system into the ferroelectric $P2_1$ phase at $T_{C2}=220$ K.[14] The complex dielectric permittivity of BPI has been investigated in a wide frequency range. Deuteration shifts the phase-transition temperature up to 300 K.[15] The structural similarity of BP and BPI allows to grow mixed BP/BPI crystals in the whole range of composition. The phase diagram of BP_xBPI_{1-x} has been investigated[16,17] by means of x-ray and pyroelectric methods. A very small amount of BP changes the ferroelectric phase transition temperature significantly. The same effect has been observed in DBP_xDBPI_{1-x}.[18] With substitution of BPI by BP already at the BP concentration $x=0.15$ the ferroelectric phase transition is suppressed and a glass-like phase-transition occurs.[8,19] Dielectric and ENDOR investigations of $BP_{0.15}BPI_{0.85}$ and $DBP_{0.15}DBPI_{0.85}$ have been performed.[8,19–21] The freezing phenomena in $BP_{0.15}BPI_{0.85}$ and $DBP_{0.15}DBPI_{0.85}$ reveal the the characteristics of a transition into a dipolar glass state with peculiarities due to the quasi-one-dimensional structure. Using the Kutnjak model[7] glass temperatures of 25 K and 10 K have been estimated for $DBP_{0.15}DBPI_{0.85}$ protonated $BP_{0.15}BPI_{0.85}$, respectively.

In this paper, the results of dielectric investigation of $BP_{0.15}BPI_{0.85}$ and $DBP_{0.15}DBPI_{0.85}$, in the region of the low-frequency dielectric dispersion are presented together with a different approach to the analysis of broad band dielectric spectra. The distribution function of the relaxation times has been extracted giving access to microscopic glass parameters which can be compared with magnetic resonance results. In the experimental section the experimental procedure is described, in Sec. III the dielectric spectra of $BP_{0.15}BPI_{0.85}$, $DBP_{0.15}DBPI_{0.85}$ are presented, in Sec. IV the mathematical formalism of the extraction of the relaxation times is explained, in Sec. V the microscopic parameters are extracted.

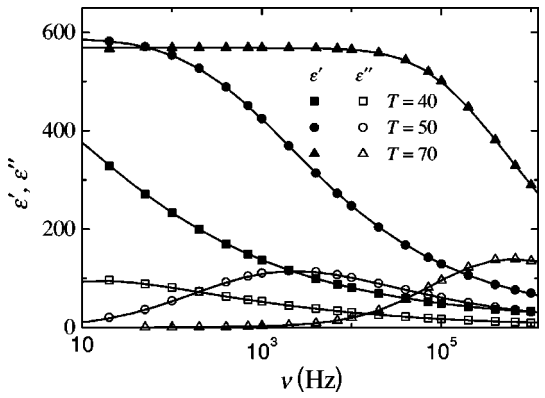

FIG. 1. The frequency dependence of ε' and ε'' at several temperatures of $DBP_{0.15}DBPI_{0.85}$ crystals. Lines are the best fits with the obtained distribution of the relaxation times.

II. EXPERIMENT

$BP_{0.15}BPI_{0.85}$ and $DBP_{0.15}DBPI_{0.85}$, crystals were grown by controlled evaporation from D_2O and H_2O solutions containing betaine with 85% of H_3PO_4 and 15% of H_3PO_3. By analogy with DBPI[15] one expects that only the protons in the O—H···O bonds of the inorganic H_3PO_4 and H_3PO_3 should be replaced by deuterons. For the dielectric spectroscopy, gold plated single crystals were oriented along the monoclinic b axis. The complex dielectric constant $\varepsilon^*=\varepsilon'-i\varepsilon''$ was measured by a capacitance bridge HP4284A in the frequency range 20 Hz to 1 MHz. The typical sample size was 50 mm^2 area and 0.7 mm thickness. The value of measurement voltage was 0.5 V. Further decrease of the measurement voltage does not change the results for the dielectric permittivity. All measurements have been performed on heating with the rate of about 0.5 K/min in the dielectric dispersion region. No differences in the value of the dielectric permittivity has been observed for cooling and heating due to the low value of the measurement field and the absence of temperature gradients in the sample. The temperature was measured with a calibrated silicon diode (Lake Shore type DT-470-DI-13). For the temperature-dependent measurements a Leybold VSK-4-320 cryostat was used.

III. RESULTS

For $BP_{0.15}BPI_{0.85}$ and $DBP_{0.15}DBPI_{0.85}$, crystals no anomaly in ε' indicating a polar phase transition can be detected down to the lowest temperatures. In the temperature region below 100 K dispersion effects dominate the dielectric response in the frequency range under study. The temperature behavior of ε' and ε'' is typical for glasses: with decreasing measurement frequency the maximum of ε' shifts to lower temperatures followed by the maximum of ε''. At fixed temperatures the frequency dependence of ε' and ε'' (e.g., see Fig. 1) provides clear evidence that the

TABLE I. Parameters from the Vogel-Fulcher analysis of the relaxation times τ for different $BP_{0.15}BPI_{0.85}$ crystals.

Crystal	$\ln(\tau_0,s)$	E_b/k(K)	T_0(K)
$BP_{0.15}BPI_{0.85}$	−27.7	394.16	5.8
$DBP_{0.15}DBPI_{0.85}$	−23.5	311.6	26.5

frequency dependence of ε'' is much broader than for Debye dispersion.

First the experimental data were fitted with the Cole-Cole formula

$$\varepsilon^* = \varepsilon_\infty + \frac{\Delta\varepsilon}{1+(i\omega\tau)^{1-\alpha_{cc}}}, \tag{1}$$

where $\Delta\varepsilon$ is the relaxator strength, τ is the relaxation time, α_{cc} is the distribution coefficient, ε_∞ is the contribution of all higher-frequency modes to the dielectric permitivity, and $\omega=2\pi\nu$ is the measurement frequency. If $\alpha_{cc}=0$ this formula reduces to the Debye formula.

The most probable relaxation time follows a Vogel-Fulcher law $\tau=\tau_0\exp\{E_b/[k(T-T_0)]\}$, where k is Boltzmann constant, with the parameters listed in Table I.

As it is possible to see from Figs. 1 and 2 the distribution of the relaxation times becomes very broad especially at low temperatures, as α_{cc} reaches the values of 0.8. At $\alpha_{cc}=0.5$ the relaxation times are already distributed over three decades. As already mentioned in the introduction, each one of the traditional models is strictly fixed with respect to the shape of the relaxation-time distribution function. The Cole-Cole formula assumes symmetrically shaped distribution of the relaxation times, but the real distribution function can be different from this. In order to get more precise information about the real relaxation-time distribution function, a special approach has been developed.

IV. RELAXATION-TIME DISTRIBUTION

We assume that the real and imaginary parts of the dielectric spectrum $\varepsilon(\nu)=\varepsilon'(\nu)+i\varepsilon''(\nu)$ can be represented as a superposition of independent individual Debye-like relaxation processes

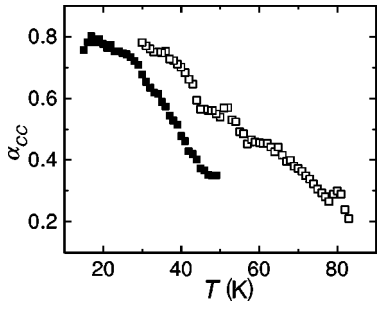

FIG. 2. The temperature dependence of the Cole-Cole distribution parameter α_{cc} for the $BP_{0.15}BPI_{0.85}$ (solid squares) and $DBP_{0.15}DBPI_{0.85}$ (open squares) crystals.

$$\varepsilon'(\nu)=\varepsilon_\infty+\int_{-\infty}^{\infty}\frac{w(\tau)d(\ln\tau)}{1+(2\pi\nu\tau)^2}, \tag{2a}$$

$$\varepsilon''(\nu)=\int_{-\infty}^{\infty}\frac{(2\pi\nu\tau)w(\tau)d(\ln\tau)}{1+(2\pi\nu\tau)^2}. \tag{2b}$$

Actually these two expressions are the first kind Fredholm integral equations for the definition of the relaxation-time distribution function $w(\tau)$. Such integral equations are known to be an ill-posed problem. The most general method of considering them is the Tikhonov regularization.[2]

Treating the integral equations (2) numerically one has to perform the discretization which leads to a linear nonhomogeneous algebraic equation set. In the matrix notation it can be represented as

$$\mathcal{A}\mathbf{X}=\mathbf{T}. \tag{3}$$

Here the components $T_n(1\leqslant n\leqslant N)$ of the vector $\mathbf{T}$ represent the dielectric spectrum $\{\varepsilon_i',\varepsilon_i''\}$ $(1\leqslant i\leqslant N/2)$ recorded at some frequency intervals ν_i. We used equidistant frequency intervals in the logarithmic scale $(\Delta\ln\nu_m=\text{const})$. The vector $\mathbf{X}$ components $X_m(1\leqslant m\leqslant M)$ stand for the relaxation-time distribution $w(\tau_m)$ that we are looking for. We used equidistant time intervals in the logarithmic scale as well $(\Delta\ln\tau_m=\text{const})$. The symbol $\mathcal{A}$ stands for the kernel of the above matrix equation. It represents the matrix with elements obtained by the direct substitution of ν_i and τ_m values into the kernels of the integral equations (2). Usually the number of data points N exceeds the number of spectrum points M. Due to the fact that Eq. (3) cannot be solved directly, it is replaced by the minimization of the following function

$$\Phi_0=\|\mathbf{T}-\mathcal{A}\mathbf{X}\|^2=\min. \tag{4}$$

Here and further we shall use the following vector norm notation $\|\mathbf{V}\|^2=\mathbf{V}^T\mathbf{V}$ where the superscript ^{T} indicates the transposed vector or matrix.

Due to the ill-posed nature of the integral Fredholm equations the above minimization problem is ill posed as well, and consequently, cannot be treated without some additional means. Thus, following the Tikhonov regularization procedure the functional Φ_0 is replaced by the modified expression

$$\Phi(\alpha)=\|\mathbf{T}-\mathcal{A}\mathbf{X}\|^2+\alpha^2\|\mathcal{R}\mathbf{X}\|^2=\min, \tag{5}$$

where an additional regularization term is added. The symbol $\mathcal{R}$ stands for the regularization matrix, and α is the regularization parameter. It plays the same role as a filter bandwidth when smoothing noisy data.

Usually there are many solutions satisfying Eq. (5) within the experimentally recorded dielectric spectrum errors. Thus, it is necessary to add as many additional conditions as possible. First, we know that all relaxation-time distribution components have to be positive $(X_n>0)$. Next, sometimes one knows rather reliable values of the static permittivity $\varepsilon(0)$ or the limit high-frequency dielectric permittivity ε_∞. In this case it is worth to restrict the above minimization problem fixing some of those values or both.

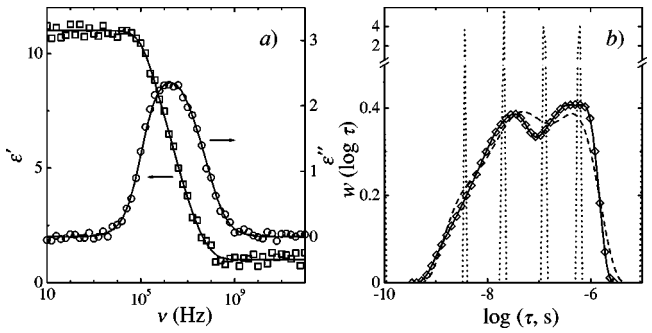

FIG. 3. The frequency dependence of dielectric permittivity (a) and corresponding relaxation-time distribution function (b). The solid lines in (a) are calculated with the corresponding initial distribution of the relaxation times shown as open diamonds in (b). The open squares in (a) are obtained by adding 3 percent random noise. The calculated distribution with different α are presented in (b): solid line $\alpha=10^{-4}$ (ϵ^* without noise), dotted line $\alpha=10^{-4}$, dashed line $\alpha=1$. (both with 3% ϵ^* noise.)

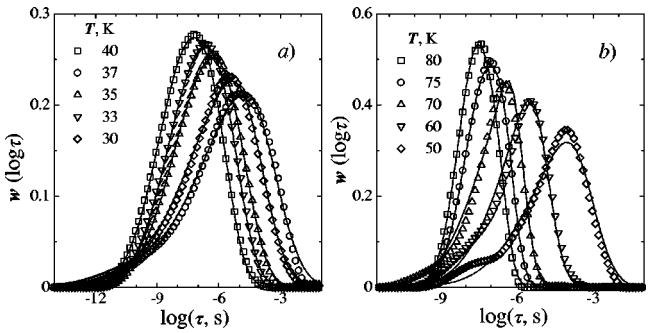

FIG. 4. The distribution function of the relaxation times at different temperatures for $BP_{0.15}BPI_{0.85}$ (a) and $DBP_{0.15}DBPI_{0.85}$ (b). Lines are the best fits with Eqs. (6), (8)–(10).

Usually the minimization problem (5) is solved numerically by means of the least squares problem technique.[22] Following the algorithm described by Provencher[23] we developed the Debye program for the numerical solution of the restricted minimization problem (5) and the calculation of the relaxation-time distribution. For the details see the Appendix.

As we used rather uniform experimental data we discarded the automatic procedures of the regularization parameter choice. Instead we performed some numerical simulations with the artificial data in order to choose most suitable parameter for our case.

Extensive simulation studies revealed that the algorithm is stable with respect to noise, provides excellent resolution of multiple relaxation processes and extracts line shapes closely approximating the true value of $w(\tau)$. An example is presented in Fig. 3. The selected starting distribution $w(\tau)$ is presented in the Fig. 3(b) with the open diamonds. From this we have calculated the frequency dependence of the real and imaginary parts of the dielectric permittivity shown as solid lines in Fig. 3(a). The reverse calculation of $w(\tau)$ from the dielectric data with the value $\alpha=0.0001$ gives exactly the same line shape [Fig. 3(b) solid line]. The added noise of 3 percent of ϵ_{max} [points in Fig. 3(a)] changes the optimal α value dramatically. As it is possible to see from the Fig. 3(b), with the value of $\alpha=0.0001$ (dotted line) the spectrum is physically meaningless, consisting of separate peaks. When $\alpha=1$ (dashed line) the shape is rather close to the real one. The main reason for the α minimum value is the quality of the measurement—or the noise of the starting data. All fits are equally good for the frequency dependence of ϵ' and ϵ''. The noise level was chosen close to the experimental accuracy.

We must note, that this method fails for the monodispersive (Debye) process, where the real distribution must be a delta function. But with noisy data, one never gets a delta distribution by means of the present formalism.

The regularization parameter α is crucial for the shape of the distribution function of the relaxation times. Too small values of α result in artificial physically meaningless structures in $w(\tau)$, while too large α tends to oversmooth the shape of $w(\tau)$ and suppress information. For the dipolar glass $BP_{0.15}BPI_{0.85}$ we have performed the serious of calculations starting from the small value of α. With α increasing the deviation between experimental and fitted spectra increases initially slowly and at certain point start to increase more rapidly. We have considered this particular value as the best.[3,23] This process revealed, that the best α value is about 1 for our experiment.

The distribution of the relaxation-times of $BP_{0.15}BPI_{0.85}$ and $DBP_{0.15}DBPI_{0.85}$ calculated from the experimental dielectric spectra at different temperatures are presented in Fig. 4 as points.

V. DISTRIBUTION OF DIELECTRIC RELAXATION-TIMES AND DIPOLAR GLASS MODEL

For the dipolar glasses it is usually assumed that the proton motion in the double well O—H$\cdots$O potentials is randomly frozenout at low temperatures, implying a static quenched disorder.[7] But due to the ''built-in'' disorder, always present in the off-stoichiometric solid solutions, there is a variety of environments for the O—H$\cdots$O bonds, leading to a distribution of the microscopic parameters of the bonds and, consequently, a distribution of dynamic properties such as the dipolar relaxation times when quenching takes place.

We consider a proton or deuteron moving in an asymmetric double-well potential. The movement consists of fast oscillations in one of the minima with occasional thermally activated jumps between the minima. Here we neglect quantum tunneling, which is negligible for deuterons although might be significant for protons at low temperatures. The oscillation frequency is ν_0. The jump probability is governed by the Boltzmann probability of overcoming the potential barrier between the minima. An ensemble of similar O—H$\cdots$O bonds has a relaxational dielectric response at lower frequencies. It was shown that the relaxation time of an individual hydrogen bond dipole in such a system[24] is given by

$$\tau=\tau_0\frac{\exp[E_b/(T-T_0)]}{2\cosh(A/2kT)}, \tag{6}$$

where $\tau_0 = 1/2\pi\nu_\infty$ with ν_∞ as the attempt frequency. This equation is similar to the Vogel-Fulcher one, except the donominator, which acounts for the asymmetry A of the local potential produced by the mean-field influence of all the other dipoles. Thus, the local polarization p (time-averaged dipole moment) of an individual O—H$\cdots$O bond is given by the asymmetry[24] parameter A

$$p = \tanh(A/2kT). \tag{7}$$

We are assuming that the parameter E_b does not change with temperature, and we are introducing the Vogel-Fulcher temperature T_0 which should effectively account for the increase of the barrier on approaching the T_0 temperature. We further consider that the asymmetry A and the potential barrier E_b of the local potential of the O—H$\cdots$O bonds both are randomly distributed around their mean values A_0 and E_{b0} according to the Gaussian law resulting in the distribution functions

$$w(E_b) = \frac{1}{\sqrt{2\pi}\sigma_E}\exp\left(-\frac{(E_b - E_{b0})^2}{2\sigma_E^2}\right) \tag{8}$$

with

$$w(A) = \frac{1}{\sqrt{2\pi}\sigma_A}\exp\left(-\frac{(A - A_0)^2}{2\sigma_A^2}\right), \tag{9}$$

where σ_E and σ_A are the standard deviations of E_b and A, respectively, from their mean values. The distribution function of relaxation-times is then given by

$$w(\ln\tau) = \int_{-\infty}^{\infty} w(A)\, w[E_b(A,\tau)]\frac{\partial E_b}{\partial(\ln\tau)}\, dA, \tag{10}$$

where $E_b(A,\tau)$ is the dependence of E_b on A for a given τ, derived from Eq. (6).

Fits with the experimentally obtained relaxation-time distributions were performed simultaneously for six different temperatures using the same parameter set: $\tau_0 = 5.58 \times 10^{-12}$ s $(1.03\times10^{-12}$ s), $T_0 = 10$ K (24.4 K), $E_{b0}/k = 392$ K (353 K), $\sigma_E/k = 49.9$ K (43.6 K), for the protonated and deuterated samples, respectively. The result is presented in Fig. 4 as solid lines. The average local potential asymmetry A_0 and the standard deviation σ_A are temperature dependent as demonstrated in Fig. 5. One can recognize the relaxation-time distribution does significantly broaden to lower temperatures. At low temperatures the relaxation-time distribution is spread out in a very wide region as it is typical for dipolar glasses. A very interesting point is that in contradiction to usual proton glasses the average asymmetry A_0 of the local potentials of the hydrogen bonds is nonzero and does disappear only for very low temperatures. From the distribution function $w(A)$ of the local potential asymmetry the distribution function $w(p)$ of the local polarizations of the hydrogen bonds can easily be deduced

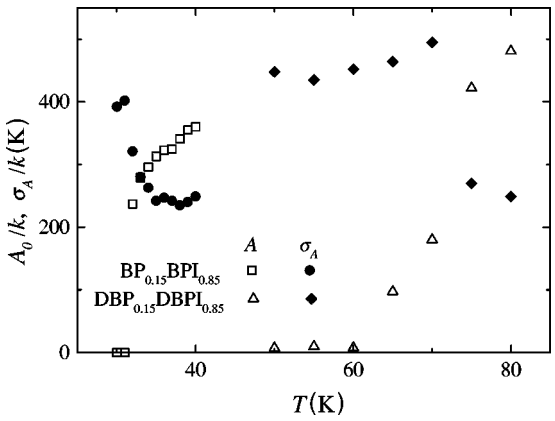

FIG. 5. Temperature dependence of the mean value A_0 (open symbols) and standard deviation σ_A (full symbols) of $BP_{0.15}BPI_{0.85}$ (□,●) and $DBP_{0.15}DBPI_{0.85}$ (△, ◆).

$$w(p) = \frac{2kT}{\sqrt{2\pi}\sigma_A(1-p^2)}\exp\left[-\frac{[\operatorname{atanh}(p) - \operatorname{atanh}(p_0)]^2}{2\sigma_A^2/(2kT)^2}\right] \tag{11}$$

which transforms in the form known for the random-bond random field (RBRF) model[25] when substituting

$$\sigma_A = 2J\sqrt{q_{EA} + \tilde{\Delta}} \tag{12}$$

and

$$A_0 = 2J_0\overline{p}. \tag{13}$$

Here, J is the Gaussian variance and J_0 the average of the random interbond coupling, $\tilde{\Delta}$ is the variance of the random local electric fields, and $\overline{p}$ the average polarization. Knowing the distribution function $w(p)$, both the average (macroscopic) polarization

$$\overline{p} = \int_{-1}^{1} p\, w(p)\, dp \tag{14}$$

and the Edwards-Anderson glass order parameter

$$q_{EA} = \int_{-1}^{1} p^2 w(p)\, dp \tag{15}$$

can be calculated.

With former electron-nuclear double resonance (ENDOR) measurements of the protonated sample,[20] the RBRF glass parameters have been determined to be $J/k = 30$ K, $J_0/k = 160$ K, and $\tilde{\Delta} = 7$ for temperatures above 90 K. Using the value $\tilde{\Delta}$ of the ENDOR results and the substitutions of Eqs. (12) and (13), the experimental parameters fitting the dielectric relaxation-time distribution deliver $J/k = 35$ K, $J_0/k = 175$ K for the protonated sample and are in good agreement with the ENDOR results. The temperature dependence of the Edwards-Anderson glass order parameter q_{EA} determined from both measurements is presented in Fig. 6. This demonstrates that besides magnetic resonance techniques the dielectric spectroscopy coupled with the data analysis pre-

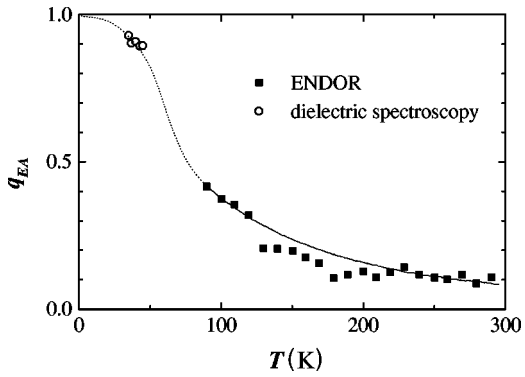

FIG. 6. Temperature dependence of the Edwards-Anderson order parameter q_{EA} for the $BP_{0.15}BPI_{0.85}$ crystals. Points above 70 K are from ENDOR results, line is guide for eye.

sented above is another appropriate tool to determine microscopic glass parameters. Because there do not exist peculiarities as such with the magnetic resonance line shape for short relaxation times, dielectric spectroscopy gives interesting results for low temperatures, especially.

Let us go back once more to the above mentioned peculiarity with the nonzero value of A_0 or J_0. As there is no evidence for a finite spontaneous polarization of our sample from hysteresis and pyroelectric measurements, the nonzero average of the local potential asymmetry must be interpreted to result from a finite average cluster polarization which is averaged out on a macroscopic scale. The cluster nature is unknown up to now. One can speculate that it is related to the strong couplings within the quasi-one-dimensional phosphite-phosphate chains $\cdots$H—O(PO)O$\cdots$H—O(PO_2)O—H$\cdots$. Further indications for a special kind of an intermediate phase between the paraelectric and glassy state from ENDOR and electron spin-lattice time measurements have already been published.[26] The new interesting result from dielectric spectroscopy is the vanishing of this cluster polarization for very low temperatures taking place for the protonated and deuterated samples at different temperatures, 30 K and 60 K, respectively. One could suspect that this disappearance of the cluster polarization is related with the real glass transition into the low-temperature nonergodic glassy phase.

VI. CONCLUSIONS

We have presented a different approach to the interpretation of dielectric spectra. The distribution of the relaxation-times have been obtained. This was performed by solving integral equation with the Tikhonov regularization technique. This method allows to extract the distribution function of the relaxation-times without any *a priori* assumptions and resolves multiple dynamical processes. As an experimental example the mixed crystals of protonated and deuterated $BP_{1-x}BPI_x$ with $x=0.85$ are presented. The dipole-freezing phenomena result in a broad asymmetrical distribution of the relaxation-times. The parameters of the double-well potentials of the hydrogen bonds, the local polarization distribution function and the glass order parameter have been extracted from the dielectric measurements. The microscopic parameters obtained are in good agreement with magnetic resonance data. The dielectric results confirm that, in opposite to usual proton glasses, dipolar clusters must exist with a nonzero electric average polarization in an intermediate phase. The interesting result from dielectric spectroscopy is the vanishing of this cluster polarization for very low-temperatures taking place for the protonated and deuterated at different temperatures, 30 K and 60 K, respectively. One could suspect that this disappearance of the cluster polarization is related with the real glass transition into the low-temperature nonergodic glassy phase.

ACKNOWLEDGMENT

This work was supported by the Lithuanian State Science foundation and Alexander von Humboldt foundation.

APPENDIX: DEBYE PROGRAM

In this section we give some details of the numerical program. Actually the program implements the simplified version of Provencher algorithm[23] adapted to the integral equation (2) case.

As it was already mentioned in Sec. IV the equidistant discretization in the logarithmic scale with steps

$$\Delta \ln \nu = h_\nu, \quad \Delta \ln \tau = h_\tau \tag{A1}$$

was used. The kernel matrix components are

$$A_{nm} = \begin{cases} h_\tau \{1+(2\pi \nu_n \tau_m)^2\}^{-1}, & n \leqslant N/2 \\ 2\pi\, \nu_n \tau_m h_\tau \{1+(2\pi \nu_n \tau_m)^2\}^{-1}, & n > N/2. \end{cases} \tag{A2}$$

When the shift ε_∞ is known and fixed, it is subtracted from data vector replacing $\varepsilon_i' \to \varepsilon_i' - \varepsilon_\infty$. In the opposite case when the shift ε_∞ is not fixed, it is added to the **X** vector as its first component. In this case the additional first $\{1, \ldots, 1, 0, \ldots, 0\}^T$ column is added to the kernel matrix.

The regularization matrix

$$\mathcal{R} = \mathcal{R}_0 = \begin{pmatrix} h_\tau^2 & 0 & 0 & 0 & \cdots & 0 \\ 1 & -2 & 1 & 0 & \cdots & 0 \\ 0 & 1 & -2 & 1 & \cdots & 0 \\ & & \cdots & & & \\ 0 & \cdots & 0 & 1 & -2 & 1 \\ 0 & \cdots & 0 & 0 & 0 & h_\tau^2 \end{pmatrix}. \tag{A3}$$

corresponding to the calculation of the second-order derivative was used. The first and last components proportional to h_τ^2 were adjusted during the simulation. In the case with not fixed shift ε_∞, value the above regularization matrix was replaced by

$$\mathcal{R} = \begin{pmatrix} h_\tau^2 & 0 \\ 0 & \mathcal{R}_0 \end{pmatrix}. \tag{A4}$$

When the static permittivity $\varepsilon(0)$ is fixed there is the additional equality condition

$$\varepsilon_\infty + \int w(\tau) d(\ln \tau) = \varepsilon(0) \tag{A5}$$

which the relaxation-time distribution has to obey. The discrete version of this condition can be presented as $\mathbf{E}^T\mathbf{X}=e$ with

$$e=\varepsilon(0)-\varepsilon_\infty, \quad \mathbf{E}^T=h_\tau\{1/2,\,1,\,\ldots,1,\,1/2\} \tag{A6}$$

in the case with fixed ε_∞, and

$$e=\varepsilon(0), \quad \mathbf{E}^T=h_\tau\{1/h_\tau^{-1},1/2,\,1,\,\ldots,1,\,1/2\} \tag{A7}$$

in the opposite case.

Thus, we have to solve the minimization problem with linear equality and inequality constraints

$$\Phi(\alpha)=\|\mathbf{T}-\mathcal{A}\mathbf{X}\|^2+\alpha^2\|\mathcal{R}\mathbf{X}\|^2=\min, \tag{A8a}$$

$$\mathbf{E}^T\mathbf{X}=e, \tag{A8b}$$

$$X_n \geqslant 0. \tag{A8c}$$

The standard way of treating such problem is the exclusion of the equality constrain, and reduction of the remaining minimization problem with inequality constraints to the LDP (Least Distance Programming) problem.[22]

The exclusion of the equality constraint is performed as follows. First, the scalar constraint (A8a) is formally replaced by its matrix analog

$$\mathcal{E}^T\mathbf{X}=\mathbf{e} \tag{A9}$$

with $M\times M$ matrix $\mathcal{E}=(\mathbf{E},0)$ and M-component vector $\mathbf{e}^T=\{e,0\}$. Next, the RQ decomposition is performed

$$\mathcal{E}=(\mathbf{K}_1\mathcal{K}_2)\begin{pmatrix} F & 0 \\ 0 & 0 \end{pmatrix}. \tag{A10}$$

Here the symbol $\mathbf{K}_1$ stands for M-component vector, and $\mathcal{K}_2$ is the $(M-1)\times M$ matrix. Those two objects together form the unitary matrix

$$\begin{pmatrix} \mathbf{K}_1^T \\ \mathcal{K}_2^T \end{pmatrix}(\mathbf{K}_1\mathcal{K}_2)=\mathcal{I}. \tag{A11}$$

Here $\mathcal{I}$ is the unity matrix.

Now inserting Eq. (A10) into condition (A9), and denoting

$$\mathbf{X}=(\mathbf{K}_1\mathcal{K}_2)\begin{pmatrix} X_1^E \\ \mathbf{X}_2^E \end{pmatrix}=\mathbf{K}_1X_1^E+\mathcal{K}_2\mathbf{X}_2^E, \tag{A12}$$

we obtain

$$X_1^E=F^{-1}e, \tag{A13}$$

and reduce the initial minimization problem to the problem with inequality constraints only

$$\Phi(\alpha)=\|(\mathbf{T}-\mathcal{A}\mathbf{K}_1F^{-1}e)-\mathcal{A}\mathcal{K}_2\mathbf{X}_2^E\|^2+\alpha^2\|\mathcal{R}\mathbf{K}_1F^{-1}e + \mathcal{R}\mathcal{K}_2\mathbf{X}_2^E\|^2=\min, \tag{A14a}$$

$$(\mathcal{K}_2\mathbf{X}_2^E)_n \geqslant -(\mathbf{K}_1)_iF^{-1}e. \tag{A14b}$$

for shorter vector $\mathbf{X}_2^E$ [with $(M-1)$ components].

The reduction of the above problem to LDP is based on the QR decomposition

$$\mathcal{A}\mathcal{K}_2=\mathcal{Q}_0\mathcal{C} \tag{A15}$$

followed by twofold singular value decompositions

$$\mathcal{R}\mathcal{K}_2=\mathcal{U}\mathcal{H}\mathcal{Z}^T, \tag{A16a}$$

$$\mathcal{C}\mathcal{Z}\mathcal{H}^{-1}=\mathcal{Q}\mathcal{S}\mathcal{W}^T. \tag{A16b}$$

Here matrices $\mathcal{Q}_0,\mathcal{U},\mathcal{Z},\mathcal{Q},\mathcal{W}$ are orthogonal ($\mathcal{Q}_0^T\mathcal{Q}_0=\mathcal{I}$, etc.), matrices $\mathcal{H}$ and $\mathcal{S}$ are diagonal with diagonal matrix elements H_n and S_n, correspondingly, and the matrix $\mathcal{C}$ is upper triangular.

The substitution

$$\mathbf{X}_2^E=\mathcal{Z}\mathcal{H}^{-1}\{\mathcal{W}\boldsymbol{\lambda}-\mathcal{U}^T\mathcal{R}\mathbf{K}_1F^{-1}e\} \tag{A17}$$

changes the minimization problem (A14) into the following one:

$$\Phi(\alpha)=\|\boldsymbol{\gamma}-\mathcal{S}\boldsymbol{\lambda}\|+\alpha^2\|\boldsymbol{\lambda}\|=\min, \tag{A18a}$$

$$(\mathcal{D}\boldsymbol{\lambda})_n \geqslant -d_n, \tag{A18b}$$

where

$$\mathcal{D}=\mathcal{K}_2\mathcal{Z}\mathcal{H}^{-1}\mathcal{W}, \tag{A19a}$$

$$\mathbf{d}=\{\mathcal{K}_2\mathcal{Z}\mathcal{H}^{-1}\mathcal{U}^T-\mathcal{I}\}\mathbf{K}_1F^{-1}e, \tag{A19b}$$

$$\boldsymbol{\gamma}=\mathcal{Q}^T\{\mathcal{Q}_0^T\mathbf{T}+(\mathcal{C}\mathcal{Z}\mathcal{H}^{-1}\mathcal{U}^T-\mathcal{Q}_0^T\mathcal{A})\mathbf{K}_1F^{-1}e\}. \tag{A19c}$$

The main advantage of the obtained minimization problem is that both functional $\Phi(\alpha)$ parts are composed of the diagonal components only. Thus, it can be easily rewritten in the single diagonal form

$$\Psi=\|\boldsymbol{\xi}\|=\min, \tag{A20a}$$

$$(\mathcal{D}\tilde{\mathcal{S}}^{-1})_n \geqslant -(\mathbf{d}+\mathcal{D}\tilde{\mathcal{S}}^{-1}\tilde{\boldsymbol{\gamma}})_n, \tag{A20b}$$

where the symbol $\tilde{\mathcal{S}}$ stands for diagonal matrix with the components $\tilde{S}_n=\sqrt{S_n^2+\alpha^2}$, $\tilde{\boldsymbol{\gamma}}$ is the vector with components $\tilde{\gamma}_n=\gamma_nS_n/\tilde{S}_n$, and

$$\boldsymbol{\lambda} = \tilde{\mathcal{S}}^{-1}(\boldsymbol{\xi} + \tilde{\boldsymbol{\gamma}}). \tag{A21}$$

The final minimization problem (A20) can be solved by LDP technique. When the vector $\boldsymbol{\xi}$ is found the vector $\mathbf{X}$ (actually the relaxation-time distribution) is obtained by means of Eqs. (A21), (A17), (A13), and (A12).

In the case when $\varepsilon(0)$ is not fixed there is no Eq. (A8a), and the algorithm is more simple. It can easily be obtained from the previous one formally assuming that $\mathbf{K}_1 = 0$ and $\mathcal{K}_2 = \mathcal{I}$.

The Debye program is written in C^{++} as a Single Document Interface program for the Windows98 environment. The LDP subroutine was rewritten from the fortran version given in,[22] the matrix decomposition subroutines were taken from.[27]

[1] R.M. Hill and A.K. Jonscher, Contemp. Phys. **24**, 75 (1983).
[2] A.V. Tichonov, Dokl. Akad. Nauk SSSR **153**, N3 (1963).
[3] H. Schäfer, E. Sternin, R. Stanarius, M. Arndt, and F. Kremer, Phys. Rev. Lett. **76**, 2177 (1996).
[4] B.G. Kim, J.J. Kim, D.H. Kim, and H.M. Jang, Ferroelectrics **240**, 249 (2000).
[5] R. Pelster, T. Kruse, H.G. Krauthäuser, and G. Nimtz, Phys. Rev. B **57**, 8763 (1998).
[6] U.T. Höchli, K. Knorr, and A. Loidl, Adv. Phys. **39**, 405 (1990).
[7] Z. Kutnjak, R. Pirc, A. Levstik, I. Levstik, C. Filipič, R. Blinc, and R. Kind, Phys. Rev. B **50**, 12 421 (1994).
[8] J. Banys, C. Klimm, G. Völkel, H. Bauch, and A. Klöpperpieper, Phys. Rev. B **50**, 16 751 (1994).
[9] I. Fehst, M. Paasch, S.L. Hutton, M. Braune, R. Böhmer, A. Loidl, M. Dörfel, Th. Narz, S. Haussühl, and G.J. McIntyre, Ferroelectrics **138**, 1 (1993).
[10] W. Schildkamp and J. Spilker, Z. Kristallogr. **168**, 159 (1984).
[11] H. Ebert, S. Lanceros-Mendes, G. Schaack, and A. Klöpperpieper, J. Phys.: Condens. Matter **7**, 9305 (1995).
[12] J. Albers, A. Klöpperpieper, H.J. Rother, and K.H. Ehses, Phys. Status Solidi B **74**, 553 (1982).
[13] H.J. Brückner, H.G. Unruh, G. Fischer, and L. Genzel, Z. Phys. B: Condens. Matter **71**, 225 (1988).
[14] J. Albers, Ferroelectrics **78**, 3 (1988).
[15] H. Bauch, J. Banys, R. Böttcher, A. Pöppl, G. Völkel, C. Klimm, and A. Klöpperpieper, Ferroelectrics **163**, 59 (1995).
[16] M.L. Santos, M.R. Chaves, A. Almeida, A. Klöpperpieper, H.E. Müser, and J. Albers, Ferroelectr. Lett. Sect. **15**, 17 (1993).
[17] M.L. Santos, J.M. Kiat, A. Almeida, M.R. Chaves, A. Klöpperpieper and J. Albers, Phys. Status Solidi B **189**, 371 (1995).
[18] J. Banys, Lith. J. Phys. **38**, 499 (1998).
[19] J. Banys, A. Kajokas, C. Klimm, G. Völkel and A. Klöpperpieper, J. Phys.: Condens. Matter **10**, 8389 (1998).
[20] H. Bauch, G. Völkel, R. Böttcher, A. Pöppl, H. Schäfer, J. Banys, and A. Klöpperpieper, Phys. Rev. B **54**, 9162 (1996).
[21] J. Banys, C. Klimm, G. Völkel, H. Schäfer, A. Kajokas, and A. Klöpperpieper, J. Phys.: Condens. Matter **12**, 201 (2000).
[22] C. L. Lawson and R. J. Hanson, *Solving Least Squares Problems* (SIAM, Philadelphia, 1995).
[23] S.W. Provencher, Comput. Phys. Commun. **27**, 213 (1982).
[24] J. Dolinsek, D. Acron, B. Zalar, R. Pirc, R. Blinc, and R. Kind, Phys. Rev. B **54**, R6811 (1996).
[25] R. Pirc, B. Tadic, R. Blinc, and R. Kind, Phys. Rev. B **43**, 2501 (1991).
[26] R. Böttcher, A. Pöppl, G. Völkel, J. Banys, and A. Klöpperpieper, Ferroelectrics **208-209**, 105 (1998).
[27] W. H. Press *et al.*, *Numerical Recipes in C* (University Press, Cambridge, 1992).